A REVIEW OF RESEARCH AT DRA ON ACTIVE AND PASSIVE CONTROL OF SHOCK WAVES

P R Ashill, J L Fulker, M J Simmons and I M Gaudet
Defence Research Agency (DRA)
Bedford, MK41 6AE, UK

Abstract

A programme of research at DRA aimed at studying shock control on aerofoils is reviewed. Wind tunnel studies of the flow over a large aerofoil model at high subsonic speeds have been used to assess various devices for controlling shock waves. These include active methods in the form of 'bumps' or 'ramps' of variable height and 'passive' devices using a ventilated surface beneath the shock wave. It is shown that active control can reduce drag by up to 20% while passive control increases drag. The data from these tests have been used to assess a CFD code known as BVGK(P). Based on the BVGK transonic aerofoil code, this method includes the facility to model passive control. After describing the experimental method and the development of BVGK(P), the paper presents and discusses comparisons between prediction and measurement. It is concluded that the method gives generally good predictions of the effect of shock control on drag and aerofoil pressure distributions.

Notation

A_{EFF}	effective area of porous surface, $= \pi d^2/4P$
c	aerofoil chord
C	constant in equation (1a), taken to be 2.4
C_D	drag coefficient
C_{Dw}	wave-drag coefficient
C_E	entrainment coefficient, $(dm_B/ds)/\rho_{iw}U_{iw}$
C_f	local skin-friction coefficient, $2\tau_w/\rho_{iw}U^2_{iw}$
C_L	lift coefficient
C_m	coefficient of pitching moment, about the 1/4c point, nose-up positive
C_N	normal-force coefficient
C_p	static pressure coefficient
d	nominal diameter of holes in porous plate
EIF	Equivalent Inviscid Flow
f	function defining higher-order terms
H	boundary-layer shape parameter, $= \delta^*/\theta$
$\bar{H}$	transformed shape parameter[17]
H_I	mass-flow shape parameter, $= (\delta - \delta^*)/\theta$
K	hole calibration constant
M	Mach number
m	mass flow through individual holes
m_B	mass flow entrained into boundary layer
P	porosity or open area ratio of porous surface
Q	flow speed corresponding to RVF wall pressure
R	Reynolds number based on aerofoil chord
RVF	Real Viscous Flow
S	equivalent source strength, $= W_{iw}/U_{iw}$
s	streamwise distance around aerofoil surface
t	depth of holes in porous surface
U, W	flow velocities in s and z directions
x	chordwise distance downstream of leading edge
Y	parameter defined in equation (1b)
z	distance normal to and from aerofoil surface
α	angle of incidence
δ	boundary-layer thickness
δ^*	boundary-layer displacement thickness
δ^*_E	equivalent displacement thickness, equation (6)
κ	flow or wall curvature, positive if the wall is concave outwards
μ, ν	viscosity and kinematic viscosity
θ	boundary-layer momentum thickness
σ	$\rho_w W_w/\rho_{iw}U_{iw}$
τ	shear stress

Suffixes

EQ	equilibrium conditions
L,T	leading and trailing edges of porous region
i	Equivalent Inviscid Flow
i,o	flow in and out of plenum
w	wall or aerofoil surface
I	inviscid
V	viscous
*	sonic conditions when applied to C_p, otherwise displacement surface

1 Introduction

The appearance of shock waves on aircraft wings at high subsonic speed marks the onset of a rapid drag rise. This drag rise has the effect of limiting the performance of the aircraft, for example by inhibiting speed, range and manoeuvrability. The rate at which the drag rises with either Mach number or angle of incidence depends on the type of wing section. For example, the drag rise can be particularly severe for some modern designs with relatively far-aft shock waves to ensure either increased lift or laminar flow over a significant part of the wing surface. Thus, for these designs, the limiting effect of shock waves on aircraft performance can be serious. Consequently, a programme of research to study methods of controlling shock waves has been underway for about four years at DRA Bedford.

At least two ways have been proposed for controlling shock strength as follows:

i) 'Active' control (Fig 1a) This form of control comprises a method for distorting or deflecting the wing surface in the region of the shock wave by 'bumps' or 'ramps'. The upstream face of the ramp induces compression waves that weaken the shock wave in the flow-field, thereby reducing wave drag[1,2,3].

ii) 'Passive' control (Fig 1b) In this method[3,4,5,6], the wing surface is ventilated in the region of the shock wave, the porous surface having a common plenum beneath it. A natural recirculation occurs between the region downstream of the shock and the lower pressure region further upstream. The resulting outward displacement of the streamlines upstream of the shock causes compression waves similar to those found with bumps or ramps.

Both types of control have been studied experimentally and theoretically in the DRA programme[1,2,3], the main aims of

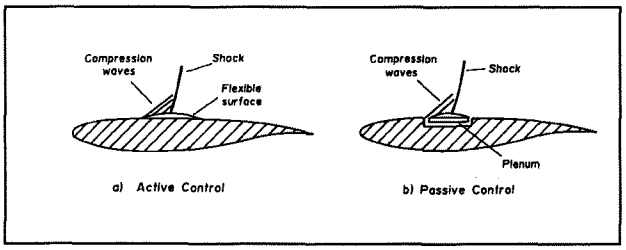

Fig 1 Shock control devices

which have been a) to investigate the drag of aerofoils with either type of control and b) to assess the accuracy of a method for predicting these flows. The experiments have been performed on aerofoils of relatively large chord (0.635m) in the 8ft x 8ft Tunnel at DRA Bedford.

After summarising the initial phases of the programme in Section 2, the paper continues with the description of the development of a CFD code for the prediction of transonic flows over aerofoils with active or passive control. For aerofoils with solid surfaces, such as those with active bump or ramp control, the transonic aerofoil code BVGK has been used to predict the flows. This code is based on the viscous/inviscid interaction principle, combining a numerical solution of the exact potential equation with integral methods for solving the boundary layer and wake equations using a semi-inverse coupling procedure[7,8]. For passive control aerofoils, it was necessary to develop the code to allow for the flow through the surface; this development, known as BVGK(P), is described in Section 3. In Section 4 the aerofoil experiments used to assess BVGK(P) both for passive and active control are described and predictions are compared with measurements in Section 5. Concluding remarks are presented in Section 6.

2 Summary of the initial phases of the programme

The programme partly arose out of a preliminary study using BVGK to assess the benefits of active control[1]. The aerofoil section used, RAE 5242, is suitable for aircraft with a significant region of Natural Laminar Flow (NLF). It has a thickness/chord ratio of 12% and other features of the shape are shown in Fig 2. Also shown is the pressure distribution at the design condition. It will be noted that transition from laminar to turbulent flow is taken at 40% on both surfaces. This position was upstream of the leading edge of any of the bumps studied.

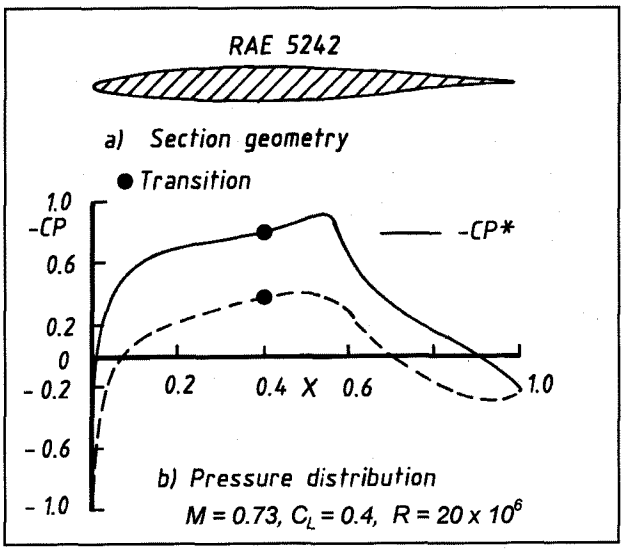

Fig 2 RAE 5242, geometry and design pressure distribution

A possible way of controlling shock strength by a flexible bump is illustrated in Fig 3. With the rear spar assumed to be at 60% chord and the flap shroud trailing edge at 78% chord it was argued that the length of the bump could be as much as 20% chord[1] and this bump length was used in the

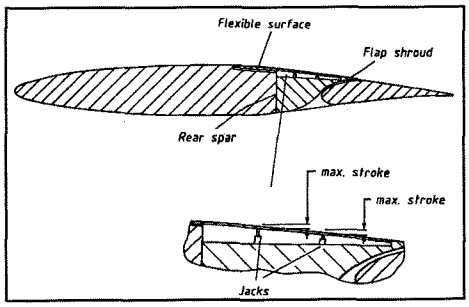

Fig 3 Possible installation of 'bump' active control

analysis. The bump shape was determined from Engineering Bending Theory assuming that the ends are built in and the surface is deflected by a point load.

Full details of the analysis are given in Ref 1 but the main conclusions are:

i) Bumps, placed in a suitable position relative to the shock wave, reduce the wave drag such that an overall reduction in drag of up to 20% can be obtained with a maximum bump deflection of 0.4% chord.

ii) These drag reductions are obtained with little change in either pitching moment or viscous drag compared with the datum case.

iii) Some increase in buffet lift coefficient is obtained with a bump for Mach numbers up to about 0.76 but, for higher Mach numbers, the effect is adverse.

With the encouragement from this initial study, work began to determine if these benefits could be achieved in wind-tunnel simulations. Plans were made to manufacture a suitable NLF aerofoil model for this purpose. It was also decided that this model should be used to assess passive control and to compare the aerodynamics of the two forms of control. Full details of this model and the experiments are given in Section 3.

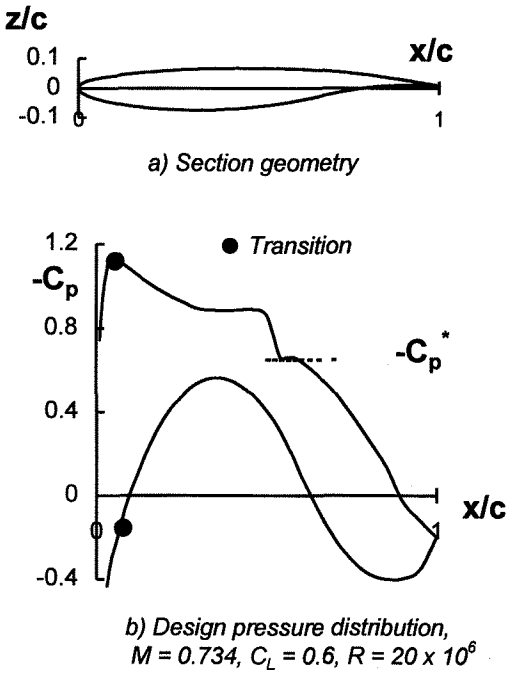

Fig 4 RAE 5225, geometry and design pressure distribution

While this work was proceeding it was decided to study in the wind tunnel the benefits of bump control on an existing aerofoil model having a 'turbulent' aerofoil section, RAE 5255. This aerofoil section is shown, along with its design pressure distribution, in Fig 4, indicating a significant degree of shock-free recompression upstream of the shock wave on the upper surface. Aerofoil flows of this type have a known tendency for the shock wave to move along the chord with changes in lift coefficient or Mach number. This is in contrast to NLF aerofoils, for which the shock wave moves slowly with free-stream conditions. This raised the possibility, therefore, that active control might only provide benefits over a limited range of Mach numbers for turbulent aerofoils. Despite this, BVGK indicated that active control would provide significant drag reductions for this aerofoil at M = 0.725 and $C_L \approx 0.7$ and so it was thought that it would be useful to perform tests on this model.

In these experiments, which are described in detail in Ref 2, the model was mounted across the working section of the 8ft x 8ft Wind Tunnel. The bumps were of circular-arc cross section; three bumps were tested, all of 20% chord length with their leading edges at 40% chord and of maximum height relative to the upper surface of the datum aerofoil of 0.125%, 0.175% and 0.25% chord. Boundary-layer transition was fixed at 5% chord on both surfaces by the air-injection method. The tests were made for Mach numbers between 0.72 and 0.74 and for two chord Reynolds numbers, 6×10^6 and 19×10^6.

At the 'design' Mach number of the aerofoils with bumps, 0.725, the predictions of pressure distributions and drag by BVGK for the datum and bump aerofoils are in reasonable agreement with experiment[9] except at lift coefficients just below the 'design' value 0.7. Here the flows showed a tendency to form a pair of shock waves on the upper surface. This may be explained by the sensitivity of these flows to small errors in Mach number. As with RAE 5242, BVGK indicated that there is no significant change in viscous drag between the datum case and the aerofoil with bump control.

The test data revealed maximum drag reductions due to the bumps similar in magnitude to those calculated for RAE 5242, but, as expected, the drag reductions were sensitive to lift coefficient and Mach number, as illustrated in Figs 5a and b.

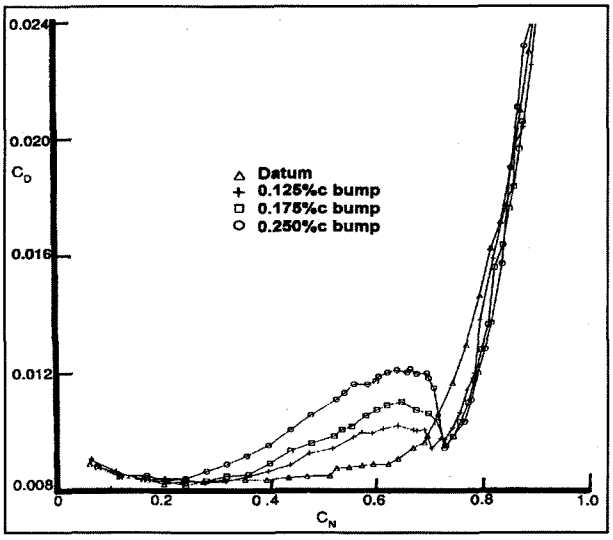

a) Variation with normal force (M= 0.725)

Fig 5 Variation of drag with normal force and Mach number

Fig 5a shows that, for lift coefficients below that at which the largest reduction is obtained, there is a large drag penalty. This arises because the aft shock wave moves upstream of the crest of the bump as lift coefficient decreases with the result that the bump increases the strength of this shock. However, at low lift coefficients, where the shock is weak and presumably wave drag is small or negligible, the bumps have little effect on drag. This suggests that, for weak shock waves at least, the bumps do not significantly affect viscous drag. The variation of the reduction in drag due to control with Mach number (Fig 5b) is consistent with the aft shock wave moving upstream with Mach number.

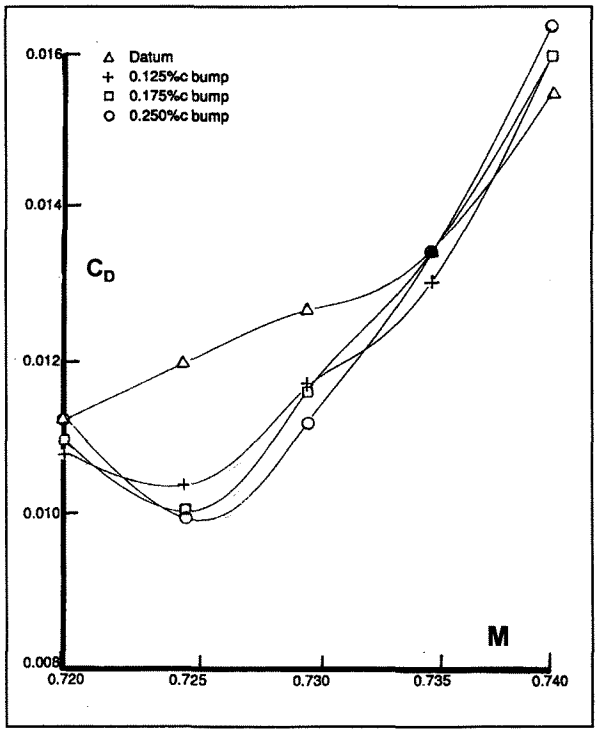

b) Variation with Mach number, $C_N = 0.75$

Fig 5 Variation of drag with normal force and Mach number

These tests suggested that active control is viable for aerofoils and provided the necessary confidence to proceed further to examine the relative benefits of active and passive control for the NLF aerofoil model and the accuracy of the predictions of them by BVGK(P).

3 Development of BVGK(P)

3.1 Basic description of method

As noted in the Introduction, the underlying method in BVGK(P) is that used in BVGK with modifications to allow for surface transpiration in the porous region of the aerofoil. In making these modifications it is assumed that the boundary layer at the porous region is fully turbulent.

A simplified flow diagram is given in Fig 6, showing the essential features of BVGK(P). As indicated, the main change is the inclusion of a module to allow for the effect of the flow through the surface. The method used to determine this surface transpiration is described in Section 3.2. Here the model of the flow through the small holes in

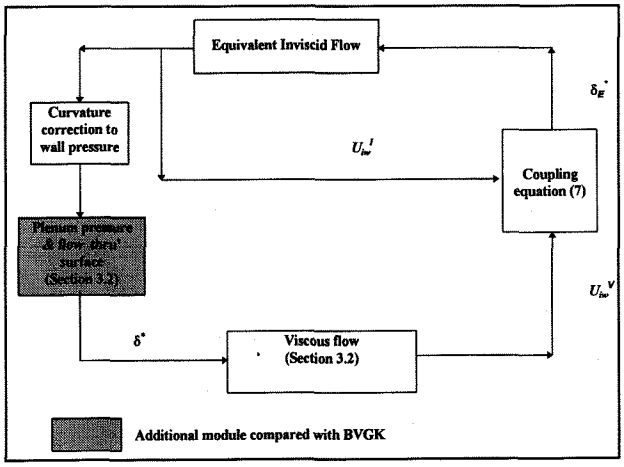

Fig 6 Simplified flow diagram of BVGK(P)

the perforated surface and the representation of this flow by an homogeneous flow are described.

The effect of the flow through the aerofoil surface on the turbulent boundary-layer development is described in Section 3.3. Here allowance for the effect of the flow through the surface on the transpiration boundary condition for the Equivalent Inviscid Flow (EIF), the streamwise and normal momentum equations, the entrainment equation and skin friction are summarised. In addition, a revision of Carter's formula[10], used to couple the viscous and inviscid parts of the flow field, is presented.

3.2 Model of ventilated-flow region

Previous authors[11] have used Darcy's law for porous material to describe the relationship between mass flow through the surface, m, and pressure drop across it Δp. However, in his study of laminar flow through holes of circular cross section, Goldstein[12] showed that the relationship is non linear. Basing their study on the analysis given by Goldstein, Poll et al[13] obtained the following relationship:

$$Y = 40.7\,(m/\mu t) + 0.81\,C\,(m/\mu t)^2 \qquad (1a)$$

where

$$Y = (\Delta p\, d^2/\rho v^2)\,(d/t)^2, \qquad (1b)$$

d is hole diameter, t is hole depth and C is a constant, which, from Goldstein's calculations, is equal to 2.4.

According to Goldstein the flow through holes with smooth entry remains laminar for values of the Reynolds number based on mean velocity and hole diameter below about 2000. However, for disturbed entry, this value drops to 280. For the cases studied in the present report the hole Reynolds number is less than 200. Thus the assumption of laminar flow in the holes appears reasonable.

Equation (1a) may be inverted to give the expression:

$$\frac{m}{\mu t} = \frac{-40.7 + \sqrt{1656.5 + 3.24CY}}{1.62C}, \qquad (2)$$

where the positive root is preferred, since the negative root gives unrealistic (negative) values of mass flow.

In wind-tunnel studies of passive control at DRA[3] and elsewhere, the holes in the perforated region of the model are laser-drilled normal to the surface. The holes are not perfectly cylindrical, and Poll et al[13] suggested that allowance could be made for this by multiplying the term Y in equation (2) by an empirical constant, K , say, which depends on the direction of the flow through the (tapered) hole.

By the nature of passive control, air passes into and out of the plenum to preserve mass flow. Since the shape of laser-drilled holes depends on the side of the plate from which the hole is drilled, the calibration constant K may not be the same for flow passing into the plenum as for flow passing into the main flow. This suggests, therefore, writing separate expressions for the two flows, the respective flows into and out of the plenum being characterised by the suffixes i and o.

As far as the flow in the region of the aerofoil surface and the plenum is concerned, the holes are regarded as isolated, i.e. they do not influence one another. On the other hand, it is assumed that the flow through the array of holes into or from the boundary layer can be simulated by a homogeneous flow normal to the aerofoil surface. This situation is illustrated in Fig 7. Thus the local mass flow per unit area of this homogeneous flow from the plenum into the main flow can be expressed as

$$\rho_w W_w = m / A_{EFF}, \qquad (3)$$

where suffix w refers to conditions at the 'wall', $A_{EFF} = \pi d^2/4P$ and P is the porosity, taken to be independent of streamwise position along the porous surface.

From considerations of mass continuity it is possible to write

$$\int_{s_L}^{s_T} \rho_w W_w ds = 0,$$

or, by using equation (3),

$$\int_{s_L}^{s_o} m_o ds - \int_{s_o}^{s_T} m_i ds = 0, \qquad (4)$$

where s is distance along the aerofoil surface, suffixes L and T referring to the leading and trailing edges of the perforated surface and $s = s_0$ being the point at which there is no flow through the surface.

If, initially, the static pressure of the main flow just above the perforated plate is assumed given, equation (4) may be expressed as

$$F(p_p) = 0, \qquad (5)$$

where the plenum pressure, p_p, is assumed to be uniform within the plenum. Equation (5) is solved for plenum pressure using the Newton-Cotes iteration method, and a crude allowance is made for compressibility by referring density and viscosity in equations (1a) and (1b) to local wall conditions in the real viscous flow over the aerofoil. Once the plenum pressure is known, the local mass flow through a given hole is determined from equation (2).

The iteration process to determine the mass flow through the porous surface is performed prior to the calculation of the viscous flow. In this process the main-flow wall pressures used are those derived from the previous inviscid iteration (Fig 6). Numerical convergence of the process is rapid.

3.3 Modifications to the treatment of the boundary layer

Fig 7 illustrates, schematically, the Real Viscous Flow (RVF) and the EIF for an aerofoil with a porous surface.

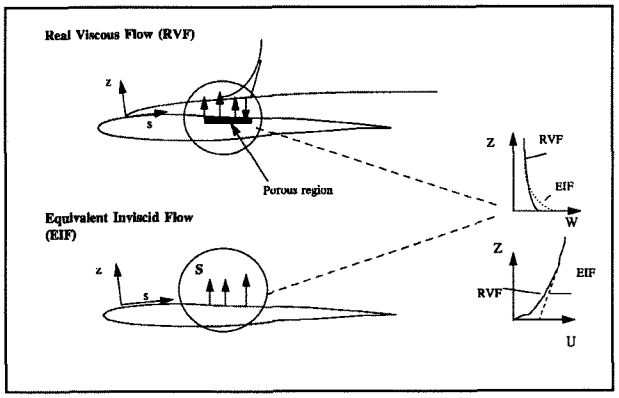

Fig 7 Real Viscous and Equivalent Inviscid Flows for aerofoil with transpiration

Allowance for the effect of flow through the aerofoil surface is made by extending East's method[14] to transpiring flows. In this method the equations of continuity and momentum of the EIF are subtracted from the corresponding equations of the RVF to form deficit

equations. These equations are then integrated normal to the aerofoil surface to the edge of the boundary layer or wake to form integral equations for the mass or momentum deficits. All the equations given below correctly reduce to the original equations for solid surfaces when the mass flow through the surface is vanishingly small.

Wall transpiration in EIF

In Ref 15 it is shown that the 'equivalent source strength'

$$S = W_{iw} / U_{iw}$$

may be expressed as

$$S = \sigma + \frac{1}{\rho_{iw} U_{iw}} \frac{d(\rho_{iw} U_{iw} \delta^*)}{ds},$$

where the suffixes *iw* refer to wall or aerofoil-surface quantities in EIF and

$$\sigma = \rho_w W_w / \rho_{iw} U_{iw}.$$

Since BVGK is based on the matching formula due to Carter[10], which uses displacement thickness, it is convenient to define an effective displacement thickness δ^*_E. This thickness is derived by integrating the expression:

$$\frac{d(\rho_{iw} U_{iw} \delta^*_E)}{ds} = \rho_{iw} W_{iw} = \sigma \rho_{iw} U_{iw} + \frac{d(\rho_{iw} U_{iw} \delta^*)}{ds}. \qquad (6)$$

along the part of the aerofoil surface where there is non-zero wall transpiration simultaneously with the integration of the other boundary layer equations.

Streamwise and normal momentum equations

After East's method is applied to the streamwise momentum equations for the two flows, the streamwise momentum integral equation may be written as[15]:

$$\frac{d\theta}{ds} = \frac{1}{(1+f)} \left(\frac{C_f}{2} + \sigma - [H + (2 - M^2_{iw})(1+f)] \frac{\theta}{U_{iw}} \frac{dU_{iw}}{ds} - \theta \frac{df}{ds} \right).$$

Here the definitions are standard except for the term f which allows for higher-order effects due to flow curvature and Reynolds normal stress terms.

In Ref 15 use is made of an approximate form of the normal momentum equation to derive the following expression for the flow speed corresponding to the wall pressure in RVF

$$Q = U_{iw}(1 + \kappa^*(\theta + \delta^*)).$$

This expression is identical to that used in BVGK except that the displacement-surface curvature κ^* is defined more generally in terms of the equivalent displacement thickness δ^*_E rather than the conventional displacement thickness δ^*.

Entrainment equation

Applying the continuity equation to the flow entering and leaving a control surface, of elementary streamwise length *ds*, that is bounded by the porous part of the aerofoil surface, it is shown in Ref 15 that

$$d(\rho_{iw} U_{iw} H_1 \theta) / ds = \rho_{iw} U_{iw} (C_E + \sigma)$$

It is shown in Ref 15 that, with the boundary layer in equilibrium,

$$(C_E)_{EQ} = \frac{H_1}{1 + f_{EQ}} \left\{ \frac{C_f}{2} + \sigma - (H + 1 + f_{EQ}) \left(\frac{\theta}{U_{iw}} \frac{dU_{iw}}{ds} \right)_{EQ} \right\} - \sigma$$

Here suffix *EQ* refers to equilibrium quantities. Green[16] presented arguments based on empirical observation for accepting that the skin-friction coefficient may be replaced by

$$C_f + 2\sigma,$$

in the 'equilibrium locus', as in the streamwise momentum equation. Thus, making use of this modification, the equation for the 'equilibrium locus' given in Ref 7 is rewritten as:

$$\left(\frac{\theta}{U_{iw}} \frac{dU_{iw}}{ds} \right)_{EQ} = \frac{1.25}{H} \left\{ \frac{C_f}{2} + \sigma - V_2 \left(\frac{\overline{H} - 1}{6.432 \overline{H}} \right)^2 (1 + 0.04 M^2_{iw})^{-1} \right\}.$$

Here V_2 is a correction for low Reynolds-number effects as defined in Ref. 7.

Departures from equilibrium are represented by the lag equation, which is used unchanged from its original form[7,17]. The relationship between the transformed shape parameter[17] $\overline{H}$ and the mass-flow shape parameter H_1 is also as used in the original method.

Skin-friction relationship

In the region of the porous surface a modified version of the skin-friction relationship is used that allows for surface transpiration. This formula relies on the work of Green[18], who based his studies on the investigation by Thompson[19] of turbulent boundary layers with suction. In common with other treatments of transpiring turbulent boundary layers[20,21] the expression for the local skin-friction coefficient, C_f, is of the form

$$C_f / C_{fs} = f(\sigma, C_{fs}),$$

where suffix s refers to the solid surface and the skin-friction coefficient is evaluated at the same values of momentum thickness Reynolds number and shape parameter as for the flow over the solid surface. Space limitations prevent the full expression being included but details can be found in Ref 15.

Coupling between the viscous and inviscid solutions

As in BVGK, the coupling between the viscous and inviscid parts of the flow is essentially that due to Carter[10]. However, the displacement thickness in this expression is replaced by the effective displacement thickness δ^*_E, since this is the one that is used to form the transpiration velocity W_{iw}. Thus Carter's equation becomes:

$$\delta_E^{*(n+1)} = \delta_E^{*n}\left(1 - \Omega(\{U^V_{iw} / U^I_{iw}\} - 1)\right) \qquad (7)$$

where superscripts I and V refer to the previous inviscid solution and to the viscous solution, n is number of (viscous) iterations and Ω is a relaxation factor.

4 Description of experiments

The wind-tunnel model, which was mounted between the sidewalls of the 8ft x 8ft Tunnel, is illustrated in Fig 8. The aerofoil section (known as RAE 5243) was of 14% maximum thickness to chord ratio and was designed to be suitable for natural laminar flow, with favourable pressure gradients on the upper and lower surfaces between the leading edge and 50% chord. In this respect the flow over the aerofoil is similar to that of RAE 5242. However, RAE 5243 is thicker than RAE 5242 and thus the design Mach number of the latter (0.68) is lower than that of the former. The use of an aerofoil with a thickness of greater than 12% was necessary for structural reasons. The chord length of the aerofoil section was 0.635m, giving a model aspect ratio of 3.84.

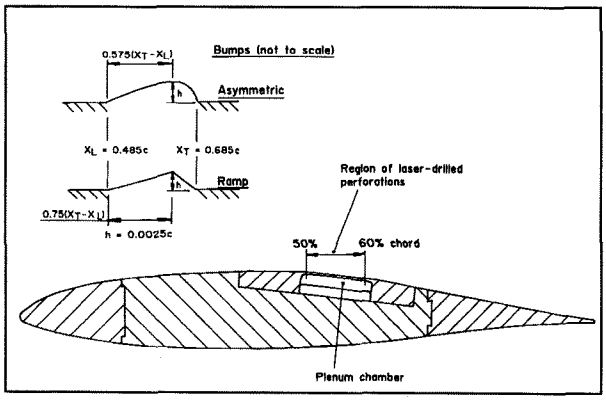

Fig 8 Aerofoil model for the study of active and passive control

Three control inserts were tested, with the passive-control type shown on the aerofoil and two 'bumps' sketched in the inset to the figure. The passive-control insert comprised a porous region extended from 50% to 60% chord on the upper surface with an open area ratio or porosity P = 0.08. The nominal diameter of the holes, d, was 0.0762 mm and the depth of the holes (or skin thickness), t, was 1 mm, giving d/t = 0.0762 and d/c = 0.00012. Calibration of the porous surface indicated that the calibration constants, K_i and K_o, are both unity[3].

The two bumps were each of maximum height of 0.25% chord, relative to the upper surface of the aerofoil. Both were of length 20% chord, with their leading edges at 48.5 % chord. One comprised a ramp while the second, referred to as the asymmetric bump, was defined by two circular arcs (Fig 8). The ramp device is of particular interest because it offers a simple way of providing control by making use of the same mechanical systems that are used for spoiler control. Further details of the geometry of these devices will be found in Ref 3.

The measurements included surface static pressures at three stations across the span, 25%, 50% and 75% span, at each of which there were 35 holes on the upper surface and 22 on the lower. However, in this paper only data measured at the centre-line station are presented. Sectional drag at mid-span was determined by applying the method of Ref 22 to measurements made with a wake rake of pitot and static tubes situated two aerofoil chords downstream of the model trailing edge.

The model was free to rotate in a bearing at one end and thus was, in principle, prone to aeroelastic twist about its flexural axis. However, wind-off calibrations made prior to the tests indicated that this twist would be negligible and it has therefore been ignored[3].

Boundary-layer transition was fixed by narrow bands of sparsely-distributed ballotini (glass balls) cemented to the model by epoxy resin placed at 5% chord on both surfaces. The width of the band was 2.5mm and the diameter of the ballotini was in the range 0.1mm to 0.13mm with a density of about 5 balls/mm^2. This ensured that boundary-layer transition was fixed at the lowest chord Reynolds number of the test, 6 x 10^6. Consequently, the boundary layer was probably 'over-fixed' at the highest test Reynolds number, and this point needs to be remembered when considering the comparisons between calculation and measurement presented below.

Since the walls of the 8ft x 8ft Tunnel are solid it is necessary to allow for wall interference. Blockage was determined using a method that makes use of wall pressures along with classical linear theory to predict the ratio of the blockage increment in velocity (say) to the

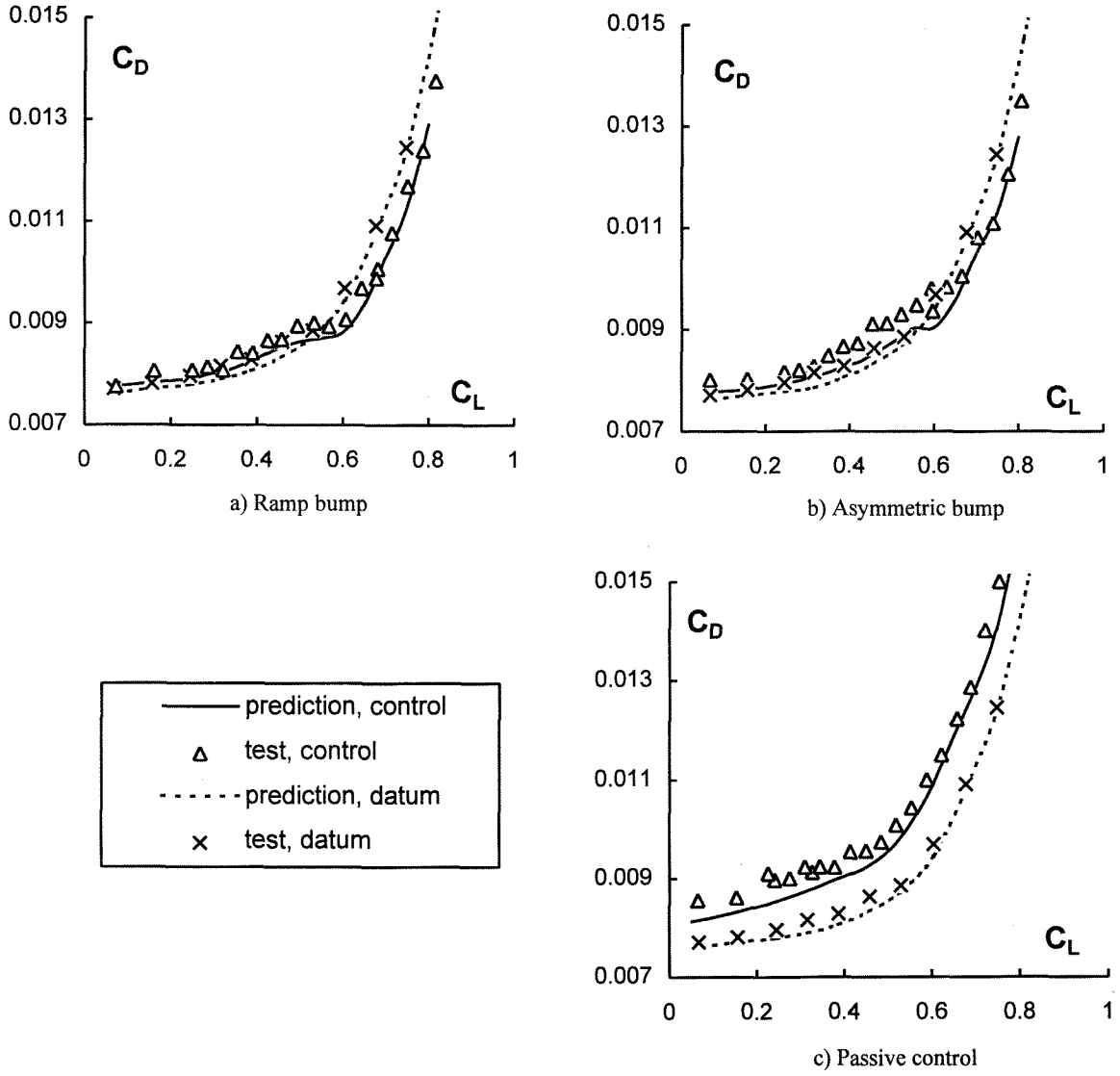

Fig 9 Comparisons between predicted and measured drag polars, M = 0.68

increment in velocity at the tunnel walls, due to the presence of the model[23]. Upwash was determined by using linear theory[24] in combination with the measured value of lift or circulation around the aerofoil.

Details of the test conditions are given in Ref 3 but, in summary, tests were performed at Mach numbers between 0.65 and 0.71 at a chord Reynolds number R = 19 x 10^6 and for Mach numbers between 0.67 and 0.70 at R = 6 x 10^6.

5 Comparisons between CFD and measurement

5.1 Calculation procedure

In the assessment of the method, the ordinates of the datum (solid surface) aerofoil and the aerofoils with control inserts are those obtained from precise inspection measurements[3]. As in previous assessments of BVGK against measurements made on aerofoil models in the 8ft x 8ft Tunnel[7,8], approximate allowance was made for the chordwise variation of wall-induced upwash by adjusting the camber of the aerofoil in the calculation..

As in BVGK, use was made of Lock's partially-conservative difference procedure[25] to provide an accurate simulation of shock strength and position. In all the calculations the quasi-conservative factor was set to 0.25. Furthermore, drag coefficient was calculated using the 'far-field' expression

$$C_D = C_{Dv} + C_{Dw},$$

where

$$C_{Dv} = 2\theta_f / c$$

and θ_f is the momentum thickness of the viscous wake far downstream of the aerofoil trailing edge. C_{Dw} is the wave-drag coefficient determined by a field method described in

Ref 7. In the modelling of the turbulent shear layers no allowance was made for the effects of flow curvature on turbulence in view of the fact that this correction is only significant for flows with separation and the flows considered in this paper are attached.

All calculations were made to a high degree of numerical convergence in both 'coarse' (80 x 16) and 'fine' (160 x 31) grids.

5.2 Results

All the comparisons to be presented are for $R = 19 \times 10^6$.

Figs 9a,b&c show comparisons between predictions by BVGK(P) and measurement for drag polars at M = 0.68. Results are shown for the aerofoils with the ramp bump (Fig 9a), the asymmetric bump (Fig 9b) and passive control (Fig 9c). On each figure results are included for the datum aerofoil for comparison. Generally, BVGK(P) underestimates the drag, although it predicts the drag rise behaviour satisfactorily for all three aerofoils. Significant improvement in agreement between prediction and measurement is obtained for the datum and passive-control aerofoils when allowance is made for the roughness effect of the transition trips[15]. However, whether or not allowance is made for this effect, BVGK(P) gives satisfactory predictions of the change in drag due to control for the ramp bump (Fig 9a). The prediction of the increase for passive control (Fig 9c) is also satisfactory except possibly at low lift. Here the roughness effect of the holes may need

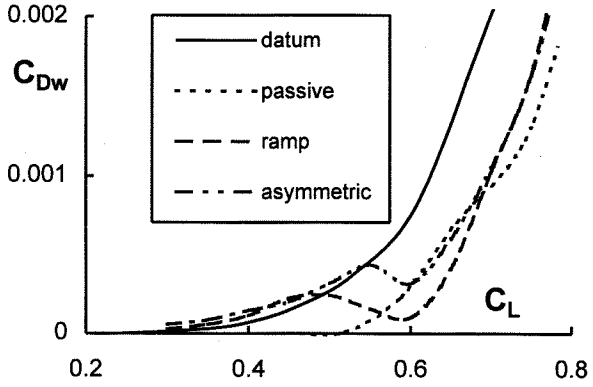

Fig 10 Predictions of wave drag, M = 0.68

to be considered. A relevant study of this problem has recently been reported in Ref 26. The ramp causes little change in drag at lift coefficients below that for drag rise. This suggests that the ramp does not significantly affect viscous drag. At higher lift coefficients the ramp reduces drag by about 12%. The asymmetric bump also provides a similar reduction in drag at lift coefficients above that for drag rise, although, in this case, the bump gives rise to a small viscous drag penalty. On the other hand, passive control increases viscous drag to such an extent that any benefits of reducing wave drag are largely offset in the range of lift coefficients considered. Analysis of data from BVGK(P) indicates that this increase results from the passive control increasing skin-friction drag in the suction region just downstream of the shock wave. This has the further effect of increasing the growth of the boundary-layer momentum thickness towards the trailing edge. A similar drag penalty due to passive control is found for the same Mach number at the lower Reynolds number 6×10^6.

Fig 10 shows comparisons of calculated wave drag for the various aerofoils at M = 0.68. For lift coefficients above about 0.5 all the devices cause a reduction in wave drag. In the case of the bumps there is an optimum lift coefficient in terms of minimum wave drag at $C_L \approx 0.6$. At this lift coefficient the shock wave is situated at between 1% and 2% chord upstream of the crest of the bump.

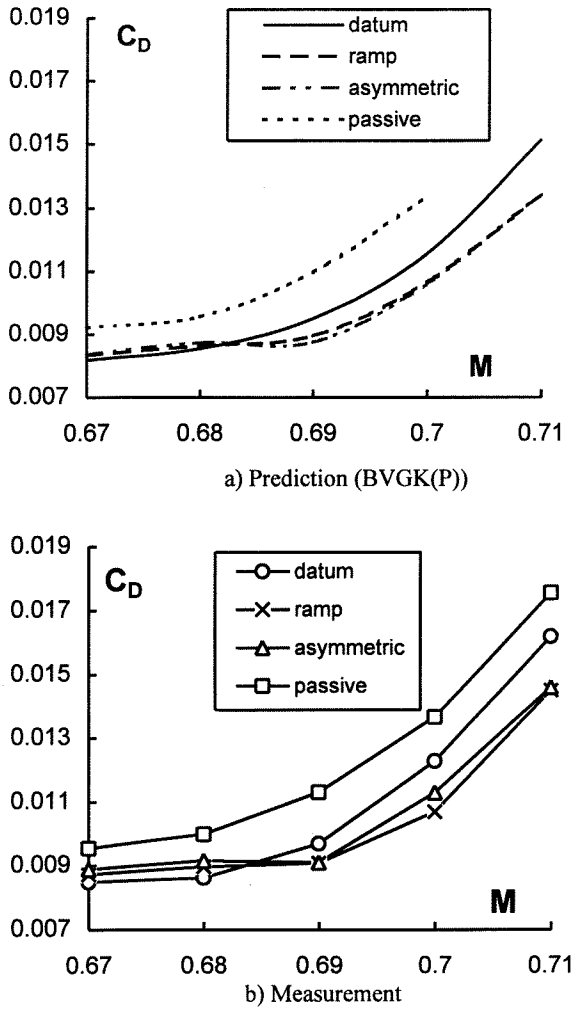

Fig 11 Variation of drag with Mach number, $C_L = 0.5$

Figs 11a&b show predicted and (interpolated) measured variations of drag coefficient with Mach number at a lift coefficient of 0.5. As before, BVGK(P) consistently

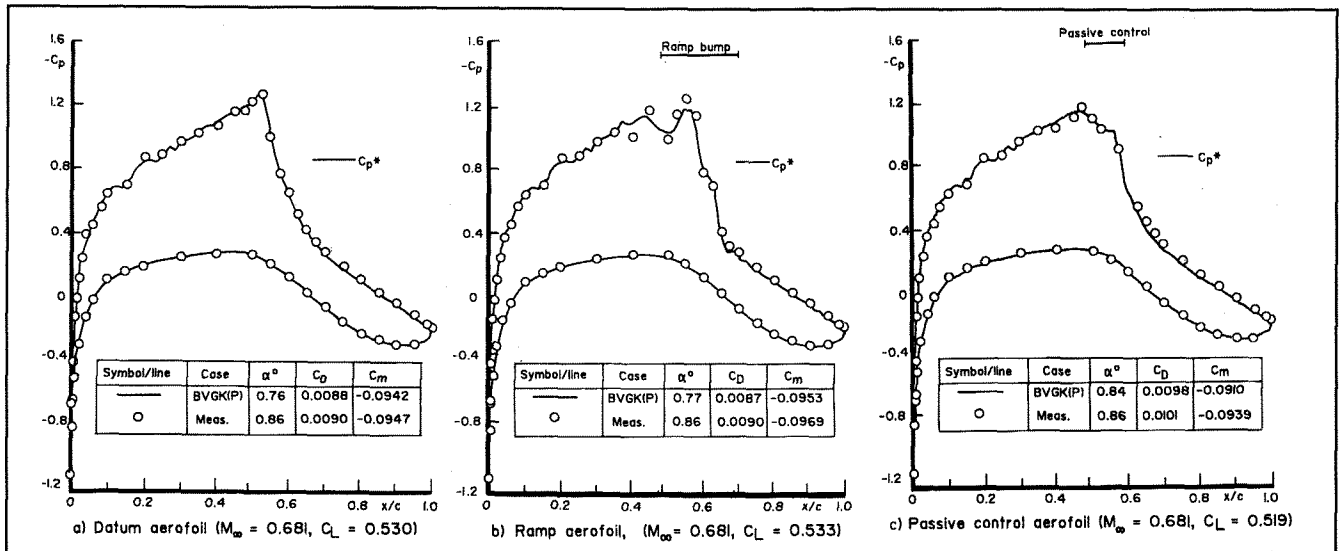

Fig 12 Comparisons of pressure distributions, M ≈ 0.68, C_L ≈ 0.52

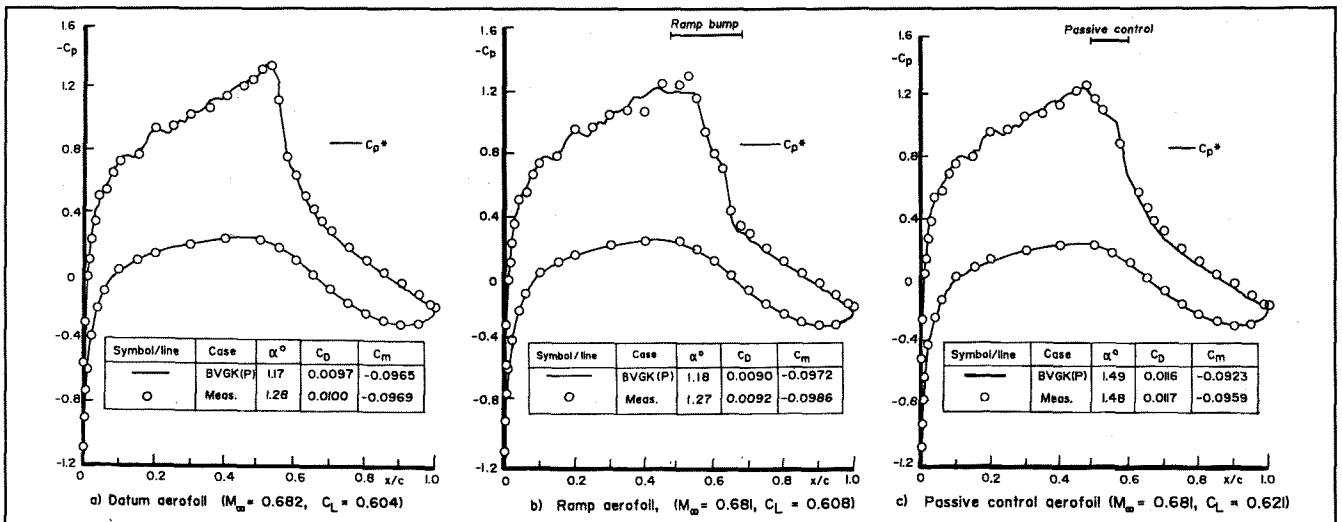

Fig 13 Comparisons of pressure distributions, M ≈ 0.68, C_L ≈ 0.62

underestimates the drag by an amount that can be explained by the roughness effect of the transition trips but the measured variation and the changes in drag due to control are both well represented by the method. As with the variations with lift coefficient shown in Figs 9a&b, the reductions in drag obtained with the bumps occur over a wider range of conditions than for the turbulent aerofoil RAE 5225. This is consistent with the position of the shock wave on the NLF aerofoil being less responsive to changes in either lift coefficient or Mach number than for the turbulent aerofoil.

The reductions in drag due to active control in these tests are lower than the maximum reductions predicted for RAE 5242 and measured for the turbulent aerofoil RAE 5225. However, the maximum bump amplitude studied in these tests was lower than in the theoretical study for RAE 5242.

Figs 12, 13 and 14 show comparisons between predicted and measured aerofoil pressure distributions at a given lift coefficient for M = 0.68 and for C_L ≈ 0.52, 0.62 and 0.72, respectively, for the datum aerofoil, ramp bump aerofoil and passive control aerofoil. Also shown on each figure are the angles of incidence (to achieve the required lift coefficient), drag coefficient and pitching moment coefficient. The agreement between prediction and measurement is generally good, although two particular exceptions to this statement may be noted:

i) BVGK(P) underestimates the suctions on the upper surface downstream of the shock wave for the passive-control aerofoil. The consequence is that the predicted pitching moment and change in pitching moment due to control is larger in the nose-down sense than that measured. This occurs despite the method giving a good

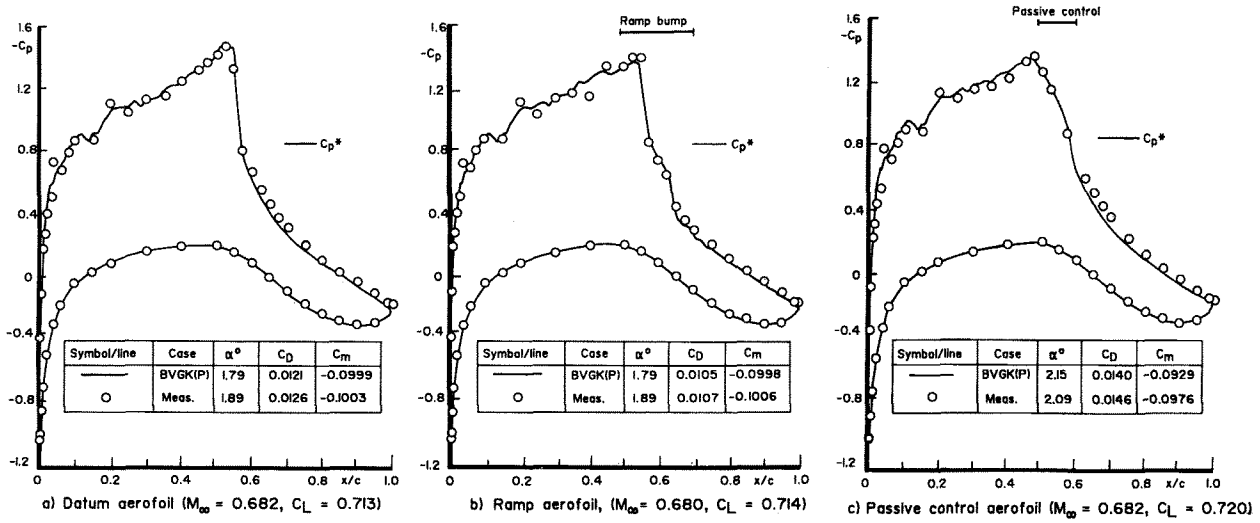

Fig 14 Comparisons of pressure distributions, $M \approx 0.68$, $C_L \approx 0.72$

representation of the pressure distribution in the region of the shock wave. This suggests that some improvements are required in the modelling of the boundary layer downstream of the porous region.

ii) The suctions just upstream of the shock wave are underestimated for the ramp-bump configuration. This may be because the method does not model properly the behaviour of the viscous-inviscid interaction where there is a discontinuity in slope.

6 Concluding remarks

This paper has reviewed CFD and wind-tunnel studies of aerofoils with shock control performed at DRA in recent years. The conclusions, in detail, are as follows:

i) Reductions of up to 20% in drag due to active (bump) control are realised for aerofoil flows with shock waves, depending on bump amplitude and position.

ii) These drag reductions are obtained because active control weakens the shock wave, thereby reducing wave drag, while not affecting boundary layer drag to any significant degree.

iii) Passive control results in an increase in drag over a wide range of lift coefficients, owing to the fact that flow through the aerofoil surface increases boundary-layer drag, offsetting any reductions in wave drag.

iv) Reductions in drag with active control are achieved without an increase in nose-down pitching moment, implying that active control does not cause a trim drag penalty.

v) The predictions by BVGK(P) of drag and pressure distributions are in generally satisfactory agreement with measurement for both active and passive control.

Thus the aims of this study, to investigate the drag of aerofoils with shock control and to assess BVGK(P), have been achieved. Furthermore the study has given encouragement to investigate the application of active control to 'smart' swept wings of both civil transport and military combat aircraft.

References

1 Ashill, P R., Fulker, J L., and Shires, A., "A novel technique for controlling shock strength of laminar-flow aerofoil sections", Paper presented to First European Forum on Laminar Flow Technology, Hamburg, Germany, March 1992.

2 Fulker, J L., Ashill, P R., and Simmons, M J., "Study of simulated active control of shock waves on aerofoil sections", DRA Technical Report TR93025, 1993.

3 Fulker, J L., and Simmons, M J., "An experimental study of shock control methods", DRA/AS/HWA/TR94007/1, 1994.

4 Krogmann, P., and Thiede, P., "Transonic shock-boundary layer control", ICAS 84-2.3.2, September 1984.

5 Thiede, P., and Krogmann, P., "Improvement of transonic aerofoil performance through passive shock/boundary-layer interaction control", IUTAM Symposium, Palaiseau, France 1985, Ed. J. Delery, Springer, Berlin, 1986.

6 Thibert, J J., Reneaux, J., and Schmitt, V., "ONERA activities on drag reduction", ICAS 90-3.6.1, September 1990.

7 Ashill, P R., Wood, R F., and Weeks, D J., "An improved, semi-inverse version of the viscous Garabedian and Korn method (VGK)", RAE TR87002, 1987.

8 Ashill, P R., "Calculation and measurement of transonic flows over aerofoils with novel rear sections", ICAS-88-3.10.2, 1988.

9 Ashill, P R., Fulker J L., and Simmons M J., "Simulated active control of shock waves in experiments on aerofoil models", Proceedings ICEFM ,Turin , July 1994.

10 Carter, J E., "A new boundary layer inviscid iteration technique for separated flows", AIAA Paper 79-1450, 1979.

11 Olling, Charles R., and Dulikravich, George S., "Porous aerofoil analysis using viscous-inviscid coupling at transonic speeds", International Journal for Numerical Methods in Fluids, Vol 7, 103-129, 1987.

12 Goldstein, S., (Ed) "Modern Developments in Fluid Dynamics", Vol 1, Oxford Clarendon Press, 1950.

13 Poll, D I A., Danks, M M., and Humphreys, B E., "The aerodynamic performance of laser drilled sheets", 92-01-028, Proceedings of the First European Forum on Laminar Flow Technology, Hamburg, March 1992.

14 East, L F., "A representation of second-order boundary-layer effects in the momentum integral equation and in viscous-inviscid interactions", RAE TR81002, 1981.

15 Ashill, P R, and Gaudet I M., "Assessment of a CFD method for transonic aerofoils with shock control", DRA/AS/HWA/CR95295/1, 1996.

16 Green, J E., "A discussion of viscous-inviscid interactions at transonic speeds", RAE , 1972.

17 Green, J E., Weeks, D J., and Brooman, J W F., "Prediction of turbulent boundary layers and wakes in compressible flow by a lag-entrainment method", ARC R&M 3791, Jan. 1973.

18 Green, J E., Unpublished ARA Report, December 1992

19 Thompson, B G J., "A three-parameter family of mean velocity profiles for incompressible turbulent boundary layers with distributed suction and small pressure gradients', ARC R&M 3622, April 1969.

20 Andersen, P S., Kays, W M., and Moffat, R J., "The turbulent boundary layer on a porous plate: an experimental study of the fluid mechanics for adverse pressure gradients", Thermosciences Division, Department of Mechanical Engineering, Stanford University Report HMT-15, May 1972.

21 Kays, W M., and Crawford, M E., "Convective heat and mass transfer", 2nd Edition, McGraw-Hill, New York, 1980.

22 Lock, C N H, Hilton, W F., and Goldstein, S., "Determination of profile drag by pitot traverse methods", ARC R&M 1970, 1940.

23 Isaacs, D., "Calibration of the RAE Bedford 8ft x 8ft Wind Tunnel at subsonic speeds, including a discussion of the corrections applied to the measured pressure distributions to allow for the direct and blockage effects due to calibration probe shape", ARC R&M 3583, Feb. 1968.

24 Garner, H C., Rogers, E W E., Acum, W E A., and Maskell, E C., "Subsonic wind tunnel wall corrections", AGARDograph 109, Oct. 1966.

25 Collyer M R., and Lock R C., "Prediction of viscous effects in steady transonic flow past an aerofoil", Aero. Qu., 30, 485, 1979.

26 Green, J E., Jenner, D E., Carberry, J. and Elliot, M., "An investigation of the roughness drag of a perforated surface beneath a turbulent boundary layer", Paper presented at ISASTI '96 Symposium, Indonesia, June 1996.

Acknowledgement

The work described in this paper has been supported jointly by the British Department of Trade and Industry and Ministry of Defence.